JOURNAL OF THE AMERICAN CHEMICAL SOCIETY

pubs.acs.org/JACS

Article

Tethered Tungsten-Alkylidenes for the Synthesis of Cyclic Polynorbornene via Ring Expansion Metathesis: Unprecedented Stereoselectivity and Trapping of Key Catalytic Intermediates

Vineet Jakhar, Digvijayee Pal, Ion Ghiviriga, Khalil A. Abboud, Daniel W. Lester, Brent S. Sumerlin, and Adam S. Veige*

Cite This: J. Am. Chem. Soc. 2021, 143, 1235−1246

Read Online

ACCESS | Metrics & More | Article Recommendations | Supporting Information

ABSTRACT: This report describes an approach for preparing tethered tungsten-imido alkylidene complexes featuring a tetra-anionic pincer ligand. Treating the tungsten alkylidyne [^{t}BuOCO]-W≡C^{t}Bu(THF)$_2$ (**1**) with isocyanates (RNCO; R = ^{t}Bu, Cy, and Ph) leads to cycloaddition occurring exclusively at the C═N bond to generate the tethered tungsten-imido alkylidenes (**6-NR**). Unanticipated intermediates reveal themselves, including the discovery of [(O$_2$C^{t}BuC═)W(η^2-(N,C)-RNCO)(THF)] (**11-R**) and an unprecedented decarbonylation product [(^{t}BuOCO)W(≡NR)(^{t}BuCCO)] (**14-R**), on the pathway to the formation of **6-NR**. Complex **11-R** is kinetically stable for sterically bulky isocyanate R = ^{t}Bu (**11-^{t}Bu**) and is isolated and characterized by single-crystal X-ray diffraction. Finally, adding to the short list of catalysts capable of ring expansion metathesis polymerization (REMP), complexes **6-NR** and **11-^{t}Bu** are active for the stereoselective synthesis of cyclic polynorbornene.

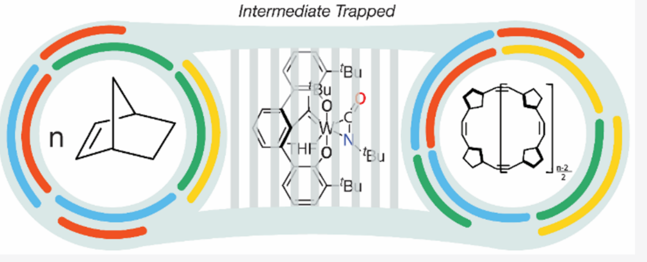

INTRODUCTION

Catalytic ring expansion metathesis polymerization (REMP)[1] is an efficient method for producing cyclic polymers from cyclic alkene monomers. REMP requires the catalyst to contain a tethered metal−carbon double bond, where the growing polymer chain remains attached to the catalyst at two points.[1−3] Employing this design strategy and a Ru-based catalyst,[4] interesting materials are now accessible, for example, cyclic dendronized polymers,[5] cyclic brush polymers,[3,6−9] and cyclic gels.[3,10]

Properties and applications unique to the cyclic topology are emerging as access to these materials increases and evidence for their cyclic topology mount.[11−15] To highlight a few, Tezuka et al. discovered enhanced thermal stability in self-assembled cyclic amphiphiles,[16,17] and Szoka et al. demonstrated greater blood circulation times for cyclic polymers, implying the potential to improve drug delivery systems.[18] Other innovative applications include using cyclic polymers to generate microscopic particles with tunable pore sizes,[19] pH responsive materials,[20] and enhancing fluorescent properties by increasing their lifetimes and emission intensity.[21,22] Exhibiting a higher T_g than its linear analog, recent reports on cyclic poly(4-methyl-1-pentene) (*c*-**PMP**) and cyclic polypropylene (*c*-**PP**) demonstrate the potential to manipulate the thermal properties of traditional polyolefins.[23,24] Possessing smaller hydrodynamic volumes than linear analogs, cyclic polymers have higher grafting densities and greater dry thicknesses on surfaces.[25] Related to the intrinsic conformational constraints of cyclic polymers and high grafting density, cyclic polymer grafted substrates exhibit low friction compared to linear grafts.[25] Imparting stereoregularity within polymers is also critical to manipulating their bulk properties, but controlling the topology (cyclic vs linear) and stereochemistry (atactic, isotactic, syndiotactic, and *cis*/*trans*) of polymers is a challenging endeavor. Only a few examples of catalysts capable of imparting stereoregularity into cyclic polymers are known.[26,27] Combining structural features to promote *Z*-selective ring-opening metathesis polymerization (ROMP)[28] with a tethered metal alkylidene,[1] we recently reported the synthesis of the tethered tungsten-oxo alkylidene (**2**) that initiates the polymerization of norbornene to yield *cis*, syndiotactic cyclic polynorbornene (>98% *cis* and syndiotactic selectivity).[26] The reaction between the trianionic (OCO^{3-}) pincer-supported tungsten-alkylidyne **1**[29] with CO$_2$ generates the tethered tungsten-oxo alkylidene **2** and the dimeric species **3** in a 9:2 ratio, respectively (Scheme 1).[26] This reaction is noteworthy not only for the generation of active catalyst **2** that

Received: December 3, 2020
Published: January 8, 2021

Scheme 1. Synthesis of Complexes 2 and 3

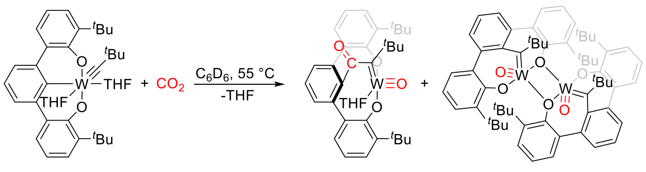

1 2 3

promotes stereoselective REMP but also for the unprecedented carbon dioxide C−O bond cleavage by an alkylidyne.

Scheme 2 outlines the proposed pathway for the formation of the tethered tungsten-oxo alkylidene.[26] The first step

Scheme 2. Proposed Pathway for the Formation of the Tungsten-Oxo Alkylidene Complex 2 Highlighting the Potential Role of the Ketenylide Intermediate

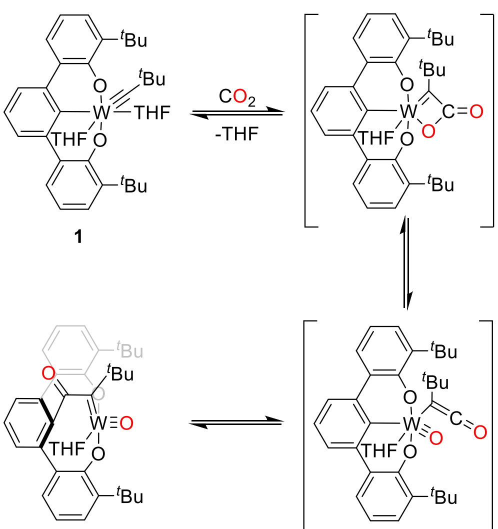

involves cycloaddition of CO_2 with complex **1** to produce an oxymetallacyclobutene intermediate followed by retrocycloaddition to form a tungsten-oxo-ketenylide. Presumably, the ketenylide moiety is unstable in the presence of the OCO^{3-} pincer ligand and inserts rapidly into the metal-aryl bond to generate complex **2**. Evidence supporting the ketenylide intermediate comes via isolation and crystallographic characterization of the related $[ONO]^{3-}$ derivative as described in Scheme 3.[30]

Carbon dioxide contains two symmetric C═O bonds, thus cycloaddition at either C═O bond results in a single product. Isocyanates (R−N═C═O) are unsymmetrical and therefore prompt the inquiry into which double bond will react

Scheme 3. CO_2 Cleavage Promoted by Complex 4 to Generate the Tungsten Oxo-Ketene Complex 5

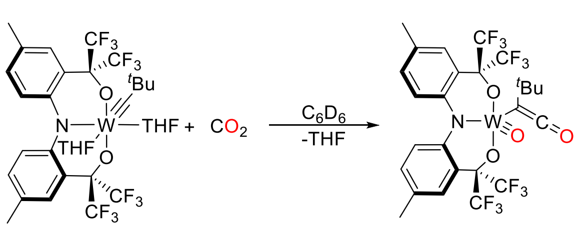

4 5

preferentially with the alkylidyne of **1**. Scheme 4 outlines the two plausible cycloaddition intermediates upon reacting with either the C═O or C═N double bond of an isocyanate. Cycloaddition with the C═O bond leads to the tethered tungsten-oxo alkylidene complex **6-O**, whereas cycloaddition with the C═N bond leads to the tethered tungsten-imido alkylidene complex **6-NR**. In **6-O**, the alkylidene bridge bears an imine, whereas in **6-NR**, the bridge contains a ketone. Employing isocyanates offers an opportunity to alter the structure of catalyst **2** by either replacing the oxo group with an imido or replacing the tethered ketone in **2** with a tethered imine, changes that can alter catalyst reactivity. Isocyanates also provide an additional site of tuning by choice of the R-group.

Previous work by Schrock et al. offers some insight into the expected reactivity of **1** with isocyanates. Treating (dme)-$Cl_3W≡C^tBu$ (dme = 1,2-dimethoxyethane) with isocyanatocyclohexane (CyNCO) yields the imido complex **7** (Scheme 5).[31] Considering the final product contains an imidocyclohexane group, this strongly suggests the reaction proceeds via [2 + 2] cycloaddition of the C═N bond across the tungsten alkylidyne to give initially a tungsten-imido-ketenylide intermediate. The ketenylide must be unstable and inserts a second isocyanate to give the final ketene product **8**. The preferential binding and cleavage of C═N compared to C═O are consistent with the strength of the double bonds in isocyanates. The C═N bond in N═C═O is weaker than C═O, both regarding its σ[32] and π[33] character, thereby promoting the cleavage of the weaker C═N bond (C═O in NCO 113.0 kJ mol^{-1}, C═N in NCO 93.4 kJ mol^{-1}, C═O in CO_2 105.8 kJ mol^{-1}).[34] From a steric perspective, the attack of the C═N bond is preferential as the two large Cy and ^{t}Bu groups are well-separated in space.

Complicating the ability to predict the reactivity of isocyanates with the trianionic pincer alkylidyne **1**, Mindiola et al. report that 2-isocyanato-2-methylpropane reacts with the niobium methylidyne (PNP)(ArO)Nb≡CH (**9**) via cycloaddition of the C═O bond instead of the C═N bond to yield the mononuclear oxo complex (PNP)(ArO)Nb═O(CH═C═N^{t}Bu) (**10**), according to Scheme 6.[35] The authors suggest steric hindrance and oxophilicity of niobium direct the selectivity.

In this work, we provide a conclusive answer for isocyanate cycloaddition regioselectivity with **1**. Cycloaddition occurs exclusively at the C═N bond to yield the imido complex **6-NR**. Additionally, during the formation of the imido complex **6-NR**, unanticipated intermediates reveal themselves, including an unprecedented decarbonylation and the discovery of an η^2-(*N*,*C*)-isocyanate complex initiator that exhibits the highest stereoselectivity (>99% *cis* and syndiotactic selectivity) for the synthesis of cyclic polynorbornene. Moreover, adding to the short list of catalysts capable of REMP, tethered tungsten-imido alkylidenes (**6-NR**) are also active catalysts for the synthesis of *cis*-syndiotactic cyclic polynorbornene.

■ RESULTS AND DISCUSSION

Cycloaddition occurs exclusively at the C═N bond to yield the imido complex **6-NR**, according to Scheme 7. However, prior to the formation of **6-NR**, the η^2-(*N*,*C*) ligated intermediate (O_2C^tBuC═)W(η^2-(*N*,*C*)-RN═C═O)(THF) (**11-R**) can be detected and, in the case of R = ^{t}Bu, isolated. **11-R** is an uncommon example of this coordination mode for a tungsten-isocyanate.[36] Treating the tungsten alkylidyne

https://dx.doi.org/10.1021/jacs.0c12248
J. Am. Chem. Soc. 2021, 143, 1235−1246

Scheme 4. Two Possible Outcomes from Cycloaddition between Complex 1 and Isocyanates (R−NCO)

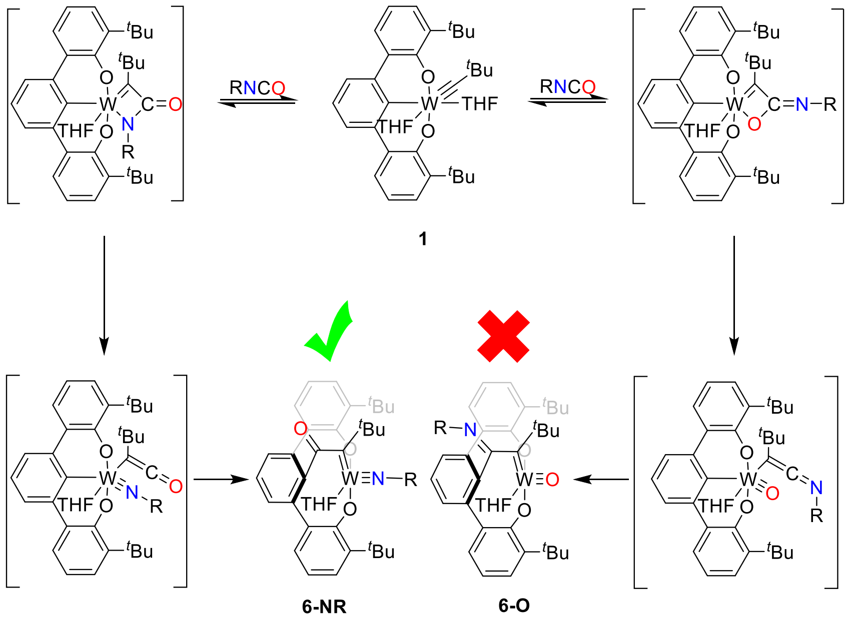

Scheme 5. Reaction of CyNCO with (dme)Cl_3WC^{t}Bu

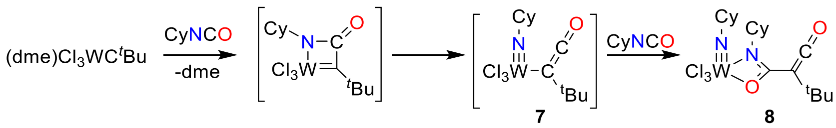

Scheme 6. Proposed Mechanisms for the Reaction of Mononuclear Niobium Methylidyne with ^{t}BuNCO

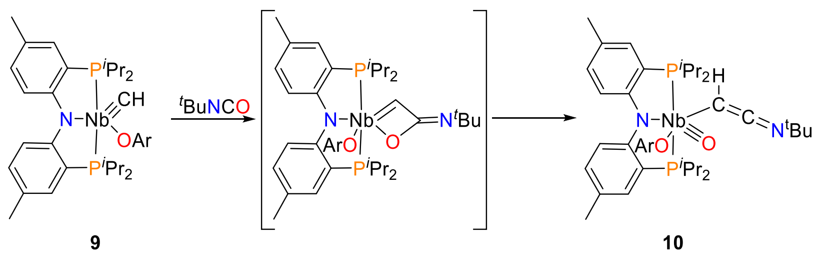

[^{t}BuOCO]W≡C^{t}Bu(THF)$_2$ (**1**) with 1 equiv of 2-isocyanato-2-methylpropane (^{t}BuNCO) in toluene-d_8 over 45 min at ambient temperature produces the tetra-anionic pincer complex (O$_2$C^{t}BuC═)W(η^2-(*N*,*C*)-^{t}BuN═C═O)(THF) (**11-^{t}Bu**) in 70% yield as a bright orange solid. In toluene-d_8, complex **11-^{t}Bu** exhibits a ^{1}H NMR spectrum indicative of C_s symmetry. Three singlets attributable to the alkylidene, pincer, and isocyanate ^{t}Bu groups resonate at 0.95, 1.39, and 1.82 ppm, respectively. In the ^{13}C{^{1}H} NMR spectrum, the alkylidene carbon (W═C) appears at 279.9 ppm, consistent with known pincer-supported tethered alkylidene complexes.[26−28,37−40] For reference, the alkylidyne carbon (W≡C) in complex **1** resonates at 320.7 ppm.[29] A resonance at 120.2 ppm for **11-^{t}Bu** corresponding to the C_{ipso} carbon indicates the central aryl ring of the pincer is not directly attached to the W(VI) metal center, as the C_{ipso}−W resonance commonly appears further downfield, around 200 ppm.[29] A ^{1}H−^{13}C gHMBC NMR spectrum optimized for a coupling constant of 3 Hz reveals the coupling over four bonds of the ^{t}Bu protons, and C_{ipso} within **11-^{t}Bu** that confirms its connectivity. Free ^{t}BuNCO exhibits a ^{13}C{^{1}H} NMR resonance at 123.6 ppm for the C atom (N═C═O). In complex **11-^{t}Bu**, the resonance appears at 202.3 ppm, confirming its η^2-(*N*,*C*) coordination to the formally W(VI) ion.[36,41] Conclusive evidence for its molecular structure comes from X-ray diffraction performed on single crystals obtained from diffusion of THF into a concentrated toluene solution of **11-^{t}Bu** at −35 °C.

Figure 1 depicts the molecular structure of **11-^{t}Bu**, and the caption lists pertinent bond lengths and angles. Complex **11-^{t}Bu** is C_s symmetric in the solid state and contains a formally W(VI) ion in a distorted octahedral geometry. The pincer ligand binds in a tetra-anionic form through two phenolate donors and an alkylidene, occupying three of the six vertices. The solid-state structure confirms that the alkylidyne originally present in complex **1** undergoes a formal reductive migratory insertion into the W-arene bond of the pincer. Similar alkylidyne insertions with complex **1** occur with alkenes and alkynes.[26−28,37−40] The η^2-(*N*,*C*) bound ^{t}BuNCO ligand and THF occupy the remaining vertices. The W═C1 bond length of 1.8755(11) Å within **11-^{t}Bu** is significantly longer than the W≡C bond length of 1.759(4) Å observed in

Scheme 7. Summary of the Synthesis of Complexes 11-R, 14-R, and 6-NR[a]

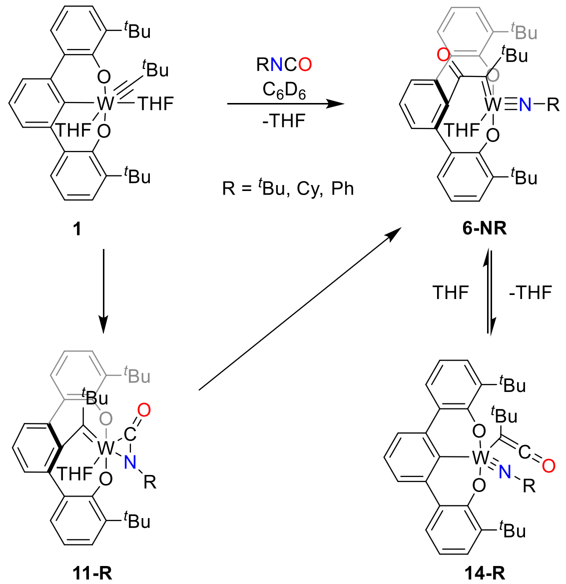

[a]R = ᵗBu, Cy, and Ph.

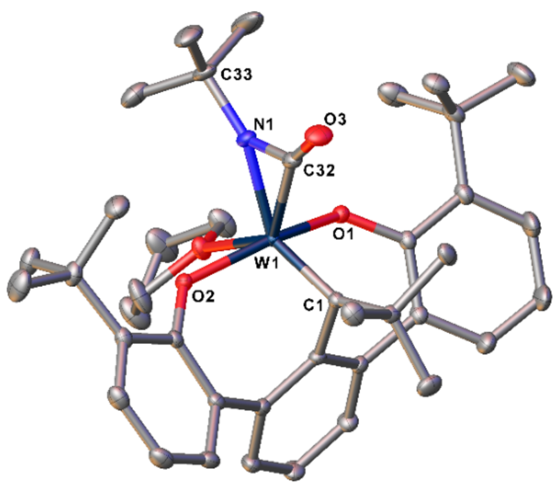

Figure 1. Solid-state molecular structure of **11-ᵗBu**. Hydrogen atoms and lattice solvent molecules (THF and toluene) are removed for clarity. Selected bond distances [Å]: W1−C1 1.8755(11), W1−N1 2.0043(10), W1−C32 2.0889(12), W1−O1 1.9655(8), W1−O2 1.9741(8), and W1−O4 2.3367(8). Selected bond angles [°]: ∠C33−N1−W1 150.31(9), ∠C1−W1−N1 127.82(4), ∠O1−W1−O2 154.06(3), ∠C1−W1−O4 134.30(4), and ∠O3−C32−W1 155.18(10).

complex **1**[29] and is comparable to other structurally characterized neutral W(VI) alkylidenes that typically range between 1.88 and 1.95 Å.[26−28,37−39] The elongated W1−O4 bond of 2.3367(8) Å for the coordinated THF suggests that it experiences a strong *trans* influence from the alkylidene and should be labile. For comparison, the THF ligands in complex **1** are labile and also have long W−O bonds (2.473(2) Å and 2.177(2) Å),[29] with the longest being *trans* to the alkylidyne. Significant π-backbonding renders the complex diamagnetic, and the bound isocyanate is best represented as a metal-laaziridinone, similar to the metallacyclopropenes observed for bound η^2-alkynes.[37−40] The N1−C32 bond (1.3278(15) Å) is significantly elongated from 1.20 Å of uncoordinated isocyanate C═N bonds.[42] Deviating significantly from linearity, the C32-N1-C33 angle in **11-ᵗBu** is 135.06(11)°, therefore providing evidence for back-donation of electron density from the tungsten center into N-C π* orbitals of the η^2-(N,C)-isocyanato ligand. The IR spectrum of **11-ᵗBu** exhibits a strong C═O stretch at 1714 cm^{-1}. Furthermore, in complex **11-ᵗBu**, the ν_{CO} band shifts by about 548 cm^{-1} in comparison to uncoordinated isocyanate C═O bonds (ν_{CO} = 2262 cm^{-1}).[43] Intermediate **11-ᵗBu** is related to Cp*M[N-(ⁱPr)C(Me)N(ⁱPr)](CO)(κ^2-*C*,*N*-OCNSiMe$_3$), where M = W and Mo, and Cp*W[N(ⁱPr)C(Me)N(ⁱPr)](CO)(κ^2-*C*,*N*-OCNᵗBu).[36]

Heating complex **11-ᵗBu** or simply combining **1** with ᵗBuNCO at 60 °C generates the tungsten-imido alkylidene complex **6-NᵗBu** in 74% yield as a bright scarlet solid. A combination of ^{1}H, ^{13}C{^{1}H}, gHSQC, and gHMBC NMR spectroscopy, combustion analysis, and X-ray diffraction studies confirms the identity of **6-NᵗBu**. Unequivocal evidence for the structure of **6-NᵗBu** comes from a single-crystal X-ray diffraction experiment performed on crystals obtained from the diffusion of pentane into a concentrated benzene solution of **6-NᵗBu** at ambient temperature. Figure 2 depicts the molecular structure of **6-NᵗBu**. The tungsten ion in **6-NᵗBu** adopts a distorted square pyramidal geometry with an Addison parameter τ = 0.30.[44] The imido group occupies the axial position, and the alkylidene, a THF ligand, and two aryloxides reside in the basal plane. A short W−N(imido) bond length (W1−N1 = 1.7302(11) Å) and a nearly linear W−N-ᵗBu angle of 164.01(10)° are consistent with a W≡N triple bond typically observed for high oxidation state tungsten-imido complexes.[45] Elongated but within the range of previously reported tetra-anionic pincer W(VI) alkylidene complexes, the W1═C1 bond length is 1.9568(13) Å.[26−28,37−39] Although not perfectly *trans* to the tungsten-alkylidene, theTHF experiences a strong *trans* influence, manifesting in a long W1−O4 bond length of 2.3023(10) Å.

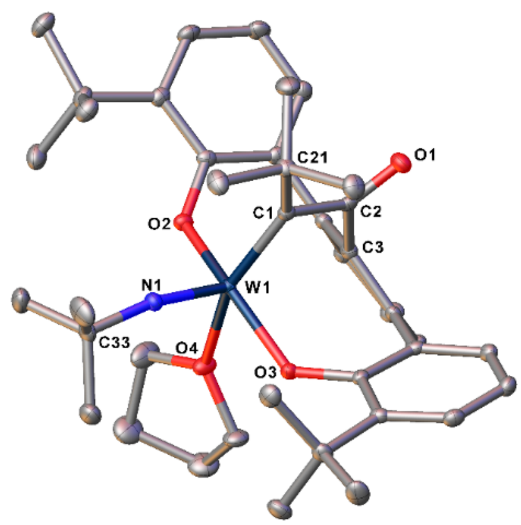

Figure 2. Solid-state molecular structure of **6-NᵗBu**. The hydrogen atoms are removed for clarity. Selected bond distances [Å]: W1−N1 1.7302(11), W1−C1 1.9568(13), W1−O2 1.9828(9), W1−O3 1.9769(9), and W1−O4 2.3023 (10). Selected bond angles [°]: ∠C33−N1−W1 164.01(10), ∠N1−W1−C1 105.58(5), ∠O3−W1−O2 150.10(4), and ∠C1−W1−O4 153.68(5).

https://dx.doi.org/10.1021/jacs.0c12248
J. Am. Chem. Soc. 2021, 143, 1235−1246

Similar to **11-^{t}Bu**, complex **6-N^{t}Bu** is also C_s symmetric in solution, as the ^{1}H NMR spectrum in toluene-d_8 displays three singlets attributable to the alkylidene, pincer, and imido ^{t}Bu groups in a 1:2:1 ratio at 1.19, 1.59, and 1.60 ppm, respectively. In the ^{13}C{^{1}H} NMR spectrum, the alkylidene carbon (W═*C*) appears at 257.3 ppm, and a resonance at 134.0 ppm corresponds to the C_{ipso} carbon. The IR spectrum of **6-N^{t}Bu** reveals a strong stretching vibration at 1569 cm^{-1} for the C═O bond. Such a feature is consistent with previously reported oxatungstacyclobutenones.[26,46] Fischer et al. report an intense band at 1645 cm^{-1},[46] and our active REMP catalyst **2** has an analogous absorption at 1588 cm^{-1}.[26] Reflecting the distinct coordination environments of **11-^{t}Bu** and **6-N^{t}Bu**, the ^{13}C{^{1}H} NMR spectra reveal some key differences. Most notable are the alkylidene carbon resonances. In complex **11-^{t}Bu**, the alkylidene carbon resonates at 279.9 ppm, whereas in **6-N^{t}Bu**, it resonates at 257.3 ppm. Similarly, the carbonyl in complex **11-^{t}Bu** resonates at 202.3 ppm, but in **6-N^{t}Bu**, it appears at 185.1 ppm. Finally, distinguishing the compounds, the ^{15}N chemical shifts are 237 ppm for **11-^{t}Bu** and 414 ppm for **6-N^{t}Bu.**

Previously reported, carbon dioxide cleavage across the metal−carbon triple bond of complex **1** occurs to give the analogous W≡O complex **2** according to Scheme 2. Considering CO_2 and isocyanates both ultimately form the tethered alkylidene, it is reasonable to expect both substrates proceed through the same reaction pathway. Lending evidence toward a ketenylide intermediate, treating a blue benzene-d_6 solution of the ONO-alkylidyne [CF_3−ONO]W≡C^{t}Bu-$(THF)_2$ (**12**)[47,48] with 1 equiv of 2-isocyanato-2-methylpropane results in a rapid color change to green, signaling the formation of the tungsten imido-ketenylide complex [CF_3−ONO]W≡N^{t}Bu(^{t}BuC═C═O) (**13**), according to Scheme 8.[30]

Scheme 8. ^{t}BuNCO Cleavage Promoted by Complex 12 to Generate the Tungsten Imido-Ketenylide Complex 13

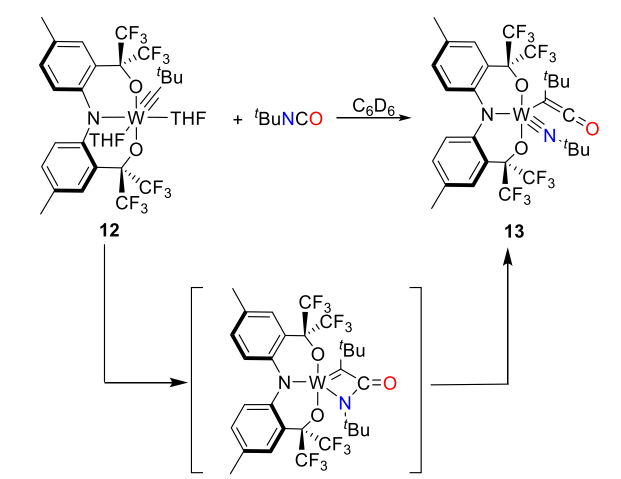

Not able to insert into the pincer W−N bond, the ketenylide is trapped. Evidence for the identity and purity of complex **13** comes from a combination of solution-phase NMR studies and solid-state structural characterization. Conclusive evidence for the complete cleavage of the C−O bond in ^{t}BuNCO comes from a single-crystal X-ray diffraction experiment performed on crystals that deposit from the diffusion of pentane into a concentrated ethereal solution of **13**. Figure 3 depicts the solid-state structure of **13**.

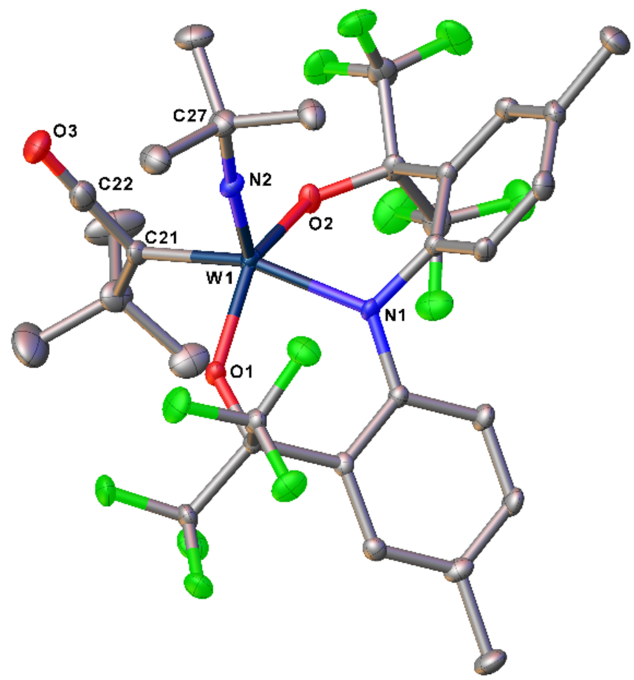

Figure 3. Solid-state molecular structure of **13**. Hydrogen atoms are removed for clarity. Selected bond distances [Å]: W1−N2 1.716(6), W1−O2 1.937(4), W1−O1 1.947(4), W1−N1 2.036(5), and W1−C21 2.059(6). Selected bond angles [°]: ∠N2−W1−O2 105.1(2), ∠N2−W1−O1 108.6(2), ∠O2−W1−O1 145.8(2), ∠N2−W1−N1 106.0(2), ∠N2−W1−C21 100.7(3), ∠N1−W1−C21 153.4(2), and ∠C27−N2−W1 175.1(5).

Data refinement reveals a structural model for **13** consistent with a C_1-symmetric complex. The W(VI) ion in complex **13** adopts a distorted square pyramidal geometry with an Addison parameter τ_5 = 0.13.[44] The imido group occupies the axial position with the pincer ligand and ketenylide moiety occupying the basal plane. The imido ligand is nearly linear, creating an angle of 175.1(5)°. A short W−N bond length (W1−N1 1.716(6) Å) and linear W−N−^{t}Bu angle are consistent with a W≡N triple bond within the range observed for tungsten-imido complexes.[45] Also, the C═O (1.168(10) Å) and C═C (1.333(10) Å) bond lengths in complex **13** are akin to known organic ketenes.[49,50] The ^{1}H NMR spectrum of complex **13** supports the assignment of a C_1-symmetric complex. For example, the methyl protons on the pincer ligand resonate as two singlets at 1.97 and 1.95 ppm. The ^{19}F{^{1}H} NMR spectrum of complex **6** is also consistent with the low symmetry, where four quartets resonate at −70.09, −70.73, −75.17, and −75.64 ppm for the CF_3 groups. More compelling evidence comes from the ^{13}C{^{1}H} NMR spectrum of complex **13** that reveals a noticeable resonance at 180.8 ppm for the ketene C═C═O carbon.[30,31,51,52] Not to be confused as simply an aromatic carbon, the assignment of the resonance as a ketenylide is also supported by IR spectroscopy;[30] an absorption appears at 2043 cm^{-1}. Confirming an imido ligand, the ^{15}N NMR chemical shift appears well-downfield at 430 ppm, whereas the pincer ligand N atom resonates at 180 ppm.

Providing compelling support for the intermediacy of a ketenylide in the formation of **6-NR** catalysts, a peculiar

https://dx.doi.org/10.1021/jacs.0c12248
J. Am. Chem. Soc. 2021, 143, 1235−1246

observation was made when monitoring a solution of **6-N^{t}Bu** on the NMR probe at 60 °C. Signals, initially thought to be an inseparable minor impurity (∼7%), appear. The signals are attributable to the ketenylide **14-^{t}Bu** (Scheme 9). Upon returning the sample to ambient temperature, signals for **14-^{t}Bu** decrease and those assigned to **6-N^{t}Bu** reappear, indicating a thermally accessible equilibrium. Critical to the transformation is the loss of THF from the coordination sphere of **6-N^{t}Bu**. Heating **6-N^{t}Bu** under vacuum results in a complete loss of THF and permits the isolation of **14-^{t}Bu** in 76% yield. Evidence for the identity of **14-^{t}Bu** comes from NMR and IR spectroscopy. Resonating at 181.7 ppm in the $^{13}C\{^1H\}$ NMR spectrum, the C═C═O of **14-^{t}Bu** matches with a previously characterized W-ketenylide (181.5 ppm)[30,31] and the structurally verified complex **13** (180.8 ppm) in Figure 3. Consistent with other complexes in this study, the ^{15}N chemical shift for the imido N atom appears downfield at 453 ppm. The IR spectrum of **14-^{t}Bu** exhibits a strong C═C═O stretching vibration at 2039 cm^{-1} that matches closely with complex **13** (2043 cm^{-1}) and with complex **5** (2050 cm^{-1}).[30] Testing the reversibility of the ketenylide insertion, addition of 1 equiv of THF to **14-N^{t}Bu** in a sealed NMR tube results in the reformation of **6-N^{t}Bu** immediately upon mixing.

Scheme 9. Equilibrium between 6-N^{t}Bu (THF Coordinated) and 14-^{t}Bu (THF Uncoordinated)

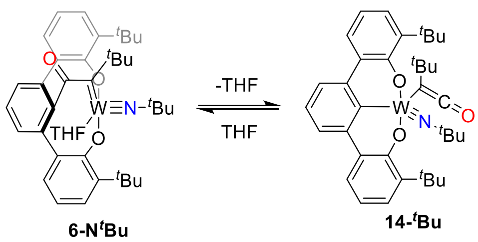

Employing CyNCO, a similar sequence of reactions occurs over 20 min to give the analogous **11-Cy** intermediate according to Scheme 7. Allowing the reaction mixture to continue at ambient temperature, **11-Cy** completely converts to **6-NCy**. Unfortunately, attempts to acquire single crystals of **11-Cy** were unsuccessful. Cooling the solution below 0 °C, however, slows the conversion of **11-Cy** to **6-NCy**, thus permitting in situ characterization by multidimensional NMR spectroscopy (see Supporting Information (SI)). The NMR data support the assignment of complex **11-Cy** as a C_s-symmetric tetra-anionic alkylidene. In the ^1H NMR spectrum of **11-Cy** (toluene-d_8, −30 °C), two singlets appear in a 1:2 ratio at 0.96 and 1.37 ppm, corresponding to the ^{t}Bu protons on the tungsten alkylidene and the ligand, respectively. In the $^1H-^{13}C$ gHMBC NMR spectrum, the alkylidene carbon (W═C) corresponds to the downfield resonance at 280.1 ppm, and a resonance at 120.3 ppm corresponds to the C_{ipso} carbon. A multinuclear $^1H-^{13}C$ gHMBC spectrum of **11-Cy** confirms the connectivity of the C_{ipso} carbon with the W═CC(CH$_3$)$_3$ protons. The complex possesses an η^2-bound CyNCO, similar to **11-^{t}Bu**. The NMR data are consistent with a η^2-(*N*,*C*) binding mode[36,41] (δ 202.5 ppm, η^2-CyN═C═O) for complex **11-Cy**. Isolated as an orange-yellow microcrystalline solid in 68% yield, complex **11-Cy** completely converts to **6-NCy** over 5 d. A combination of NMR spectroscopy, single-crystal X-ray diffraction, combustion analysis, ESI-MS, and FTIR confirm the identity of **6-NCy** (see SI).

Unequivocal evidence for the structure of **6-NCy** comes from a single-crystal X-ray diffraction experiment performed on crystals that deposit from a concentrated solution in benzene-d_6 at room temperature (Figure 4). The asymmetric unit of **6-NCy** comprises the W complex and a half benzene solvent molecule (located on an inversion center).

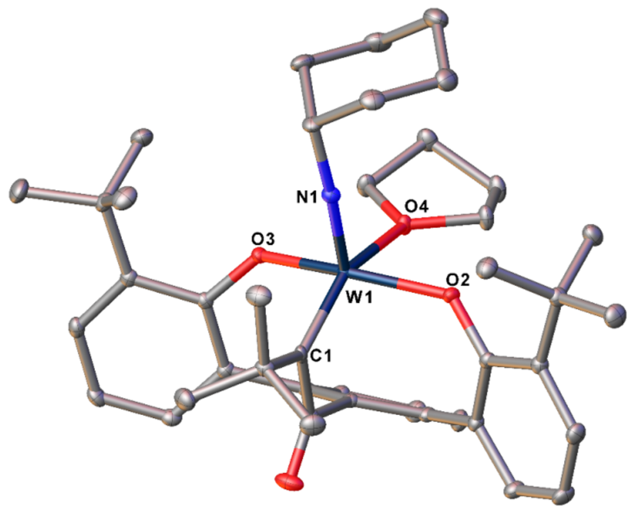

Figure 4. Solid-state molecular structure of **6-NCy**. Hydrogen atoms and lattice solvent molecule (*n*-pentane) are removed for clarity. Selected bond distances [Å]: W1−N1 1.7262(14), W1−C1 1.9601 (16), W1−O2 1.9826(11), W1−O3 1.9906(11), and W1−O4 2.2700 (12). Selected bond angles [°]: ∠C33−N1−W1 169.00(12), ∠N1−W1−C1 103.48(7), ∠O2−W1−O3 153.09(5), and ∠C1−W1−O4 152.14(6).

The size of the isocyanate substituent determines if the intermediate η^2-(*N*,*C*) complex is isolable prior to the formation of the final imido complex. Treating 1 equiv of isocyanatobenzene with 1 equiv of alkylidyne [^{t}BuOCO]W≡C^{t}Bu(THF)$_2$ (**1**)[29] in toluene-d_8 at −30 °C yields **11-Ph** and **6-NPh** in a 3:2 ratio, as determined by ^1H NMR spectroscopy. Allowing the reaction mixture to continue at ambient temperature, **11-Ph** completely converts to **6-NPh** over 3 d and is isolated as a bright red solid in 81% yield. Unfortunately, attempts to obtain single crystals of **11-Ph** were unsuccessful owing to the presence of **6-NPh**. Cooling the solution below 0 °C slows the conversion of **11-Ph** to **6-NPh**, thus permitting in situ characterization. The NMR data support the assignment of **11-Ph** as a C_s-symmetric tetra-anionic alkylidene complex similar to **11-^{t}Bu** and **11-Cy** (see SI). Evidence for the purity and identity of complex **6-NPh** comes from NMR spectroscopy and combustion analysis. Importantly, crystals amenable to single-crystal X-ray diffraction deposit from a concentrated THF solution of **6-NPh** at −35 °C layered with pentane via diffusion. Figure 5 depicts the molecular structure of **6-NPh**.

REMP and Evidence for Stereoselectivity. In catalytic REMP, even small changes to the metal complex can cause profound differences in activity.[4] For instance, the tethered tungsten-imido alkylidene complexes (**6-NR**) display lower activity for the generation of *cis*-syndiotactic cyclic polynorbornene compared to the tethered tungsten-oxo alkylidene (**2**).[26] Similarly, the activities of the tethered tungsten imido complexes (**6-NR**) increase in the order R = Cy < Ph < ^{t}Bu. The tungsten-imido complexes (**6-NR**) exhibit a strong catalytic activity dependence on the lability of the bound

https://dx.doi.org/10.1021/jacs.0c12248
J. Am. Chem. Soc. 2021, 143, 1235−1246

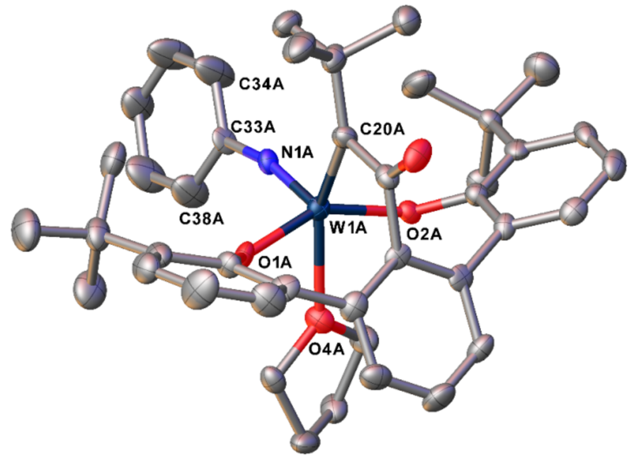

Figure 5. Solid-state molecular structure of **6-NPh**. Hydrogen atoms, W complexes B and C, and lattice solvent molecule (*n*-pentane and THF) are removed for the clarity. Selected bond distances [Å]: W1A–N1A 1.747(5), W1A–C20A 1.952(6), W1A–O1A 1.936(4), W1A–O2A 1.962(4), and W1A–O4A 2.274(4). Selected bond angles [°]: ∠C33A–N1A–W1A 166.3(5), ∠N1A–W1A–C20A 104.2(2), ∠O1A–W1A–O2A 149.77(15), and ∠C20A–W1A–O4A 153.3(2).

THF. Comparison of the W1–O4 bond length for complexes **6-NR** validates this: The bond lengths (W1–O4) increase in the same order as the polymerization activity, from 2.2700(12) Å (**6-NCy**) to 2.274(4) Å (**6-NPh**) to 2.3023(10) Å (**6-N^{t}Bu**). Catalyst **6-N^{t}Bu** exhibits the highest activity, and the activity decreases significantly upon the addition of 1 equiv of THF, suggesting that excess THF suppresses the coordination of norbornene, thereby hindering REMP. For brevity, the ensuing discussion on polymer characterization and tacticity analysis will be limited to *cis*-syndiotactic cyclic polynorbornene generated by **6-N^{t}Bu**.

Complex **6-N^{t}Bu** is an active catalyst for the stereoselective REMP of norbornene to give cyclic polynorbornene (Scheme 10; Table 1). Treating a solution of norbornene (50.0 mg, 100 equiv) in toluene with **6-N^{t}Bu** (4.23 mg, 1 equiv) for 4 h at 60 °C results in the formation of cyclic polynorbornene in 67% yield with high *cis*-selectivity. ^{1}H and ^{13}C NMR spectra are consistent with *cis*-syndiotactic polynorbornene (>95% *cis*, >97% syndiotactic).[53−56] The identification of specific trends in the polymerization results is challenging, potentially due to the rapid increase in viscosity that occurs shortly after catalyst addition. One clear observation is that a high molecular weight polymer *cis*-polynorbornene is produced under all of these conditions.

Scheme 10. Polymerization of Norbornene by Catalyst 6-N^{t}Bu to Generate Stereoregular Cyclic Polynorbornene

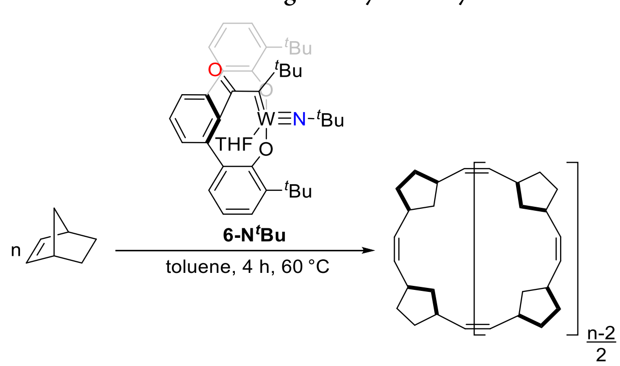

Table 1. Polymerization of Norbornene[a] by Catalyst 6-N^{t}Bu with Different Monomer/Catalyst Ratios

$[mon]/[cat]_0$	$[mon]_0$[b]	yield (%)	% *cis*[c]	M_n[d] (kDa)	M_w/M_n[d]
50:1	0.25	75	95	1940	1.53
100:1	0.25	67	95	633	3.23
200:1	0.25	42	94	677	3.19
400:1	0.25	27	95	727	2.45

[a]The appropriate amount of a catalyst solution in toluene (10 mg/mL) is added to norbornene (50 mg) dissolved in toluene and stirred for 4 h at 60 °C. [b]mol L^{-1}. [c]Determined by ^{1}H NMR spectroscopy. [d]Determined by SEC using dichlorobenzene as the mobile phase at 140 °C with a conventional calibration based on narrow polystyrene standards.

Considering the additional strain in the tethered alkylidene of complex **11-^{t}Bu** relative to **6-NR** (R = ^{t}Bu, Ph and Cy), **11-^{t}Bu** was tested for its activity in the REMP of norbornene and was found to be even more active and more selective. Treating **11-^{t}Bu** with norbornene in toluene at ambient temperature yields *cis*-selective (>99% by ^{1}H NMR spectroscopy) cyclic polynorbornene after 1 h (Scheme 11, Table 2).

Scheme 11. Polymerization of Norbornene by Catalyst 11-^{t}Bu to Generate Stereoregular Cyclic Polynorbornene

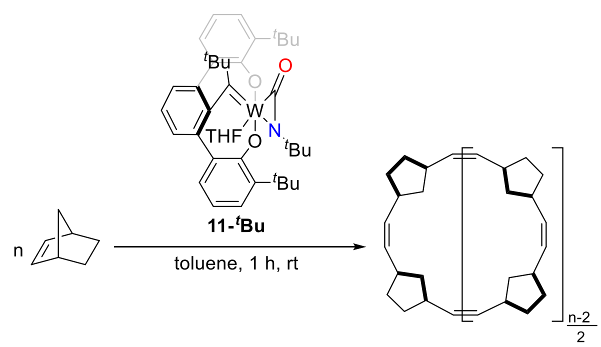

Table 2. Polymerization of Norbornene[a] by Catalyst 11-^{t}Bu with Different Monomer/Catalyst Ratios

$[mon/cat]_0$	$[mon]_0$[b]	yield (%)	% *cis*[c]	M_n[d] (kDa)	M_w/M_n[d]
50:1	0.25	95	99	436	2.02
100:1	0.25	93	99	546	3.61
200:1	0.25	80	99	458	2.09
400:1	0.25	64	99	1499	2.11

[a]The appropriate amount of a catalyst solution in toluene (10 mg/mL) is added to norbornene (50 mg) dissolved in toluene and stirred for 1 h at ambient temperature. [b]mol L^{-1}. [c]Determined by ^{1}H NMR spectroscopy. [d]Determined by SEC using dichlorobenzene as the mobile phase at 140 °C with a conventional calibration based on narrow polystyrene standards.

Adding the reaction mixture into a 10-fold excess of stirring methanol stops the polymerization and precipitates the polymer. Vacuum filtration followed by drying under vacuum overnight affords white cyclic polynorbornene. Cyclic polynorbornene produced with catalyst **11-^{t}Bu** is syndiotactic (>99%), as determined by comparison to ^{13}C NMR data of previously reported syndiotactic linear polynorbornene.[53−56] Postpolymerization modification of polynorbornene via partial bromination of the double bonds, as reported by Schrock et

https://dx.doi.org/10.1021/jacs.0c12248
J. Am. Chem. Soc. 2021, 143, 1235−1246

al.,[56] confirms the syndiotacticity of the cyclic polynorbornene. The brominated polymer displays two doublets at 3.84 ppm (J = 9.6 Hz) and 3.81 ppm (J = 9.6 Hz) (Figure S89, top). Concordant with reported *cis*, syndiotactic linear polynorbornene, irradiating the methine proton at 2.61 ppm, results in two singlets (Figure S89, bottom).[56] In addition, the FTIR spectrum of the cyclic polynorbornene exhibits a strong IR absorption at 732 cm^{-1} (*cis* out of plane = C−H bending) and a weak absorption at 1405 cm^{-1} (*cis* in-plane = C−H bending), characteristic of *cis* olefins.[57] Within minutes of adding **11-^{t}Bu** to the solution of monomer, a high viscosity is observed. The polymerization results listed in Table 2 clearly indicate that high M_n polymers are produced under all the conditions considered.

Complex **6-NPh** is also an active catalyst for the stereoselective REMP of norbornene to give cyclic polynorbornene (Scheme 12). In a typical reaction, to a 20 mL glass vial

Scheme 12. Polymerization of Norbornene by Catalyst 6-NPh to Generate Stereoregular Cyclic Polynorbornene

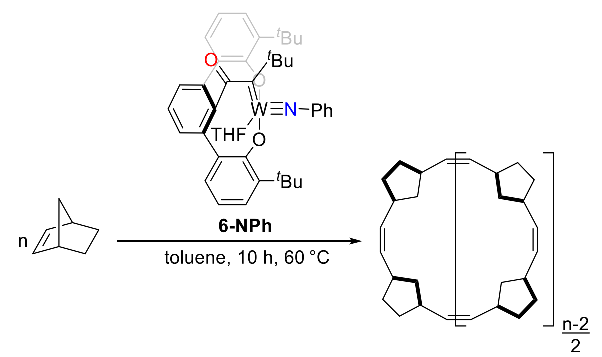

charged with norbornene (67.0 mg, 400 equiv) in 1 mL of toluene was added 145 μL of a 10 mg/mL solution of **6-NPh** in toluene (1.45 mg, 1 equiv). The reaction was allowed to stir for 10 h at 60 °C. After this period, the reaction vessel was withdrawn from the glovebox, and the reaction mixture was added dropwise to stirring methanol. Polynorbornene precipitated as a white solid that was filtered and dried overnight under vacuum. ^{1}H and ^{13}C NMR spectra are consistent with *cis*-syndiotactic polynorbornene.

Table 3 lists the results of the polymerizations as a function of [monomer]:[catalyst] ratio. As observed for the other catalysts, the polymers produced with **6-NPh** have high molecular weights, though the dispersities are lower and more consistent. Samples from these polymerizations were suitably soluble, thus allowing an interrogation of the cyclic topology.

Table 3. Polymerization of Norbornene[a] with Catalyst 6-NPh with Different Monomer/Catalyst Ratios

$[mon/cat]_0$	$[mon]_0$[b]	yield (%)	% *cis*[c]	M_n[d] (kDa)	M_w/M_n[d]
63:1	0.1	90	94	185	1.55
100:1	0.1	89	92	384	1.31
171:1	0.1	80	93	167	1.20
400:1	0.1	76	92	178	1.34

[a]The appropriate amount of a catalyst solution in toluene (10 mg/mL) is added to norbornene dissolved in toluene and stirred for 10 h at 60 °C. [b]mol L^{-1}. [c]Determined by ^{1}H NMR spectroscopy. [d]Determined by SEC using THF as the mobile phase at 35 °C equipped with MALS detection.

Size exclusion chromatography (SEC) equipped with multi-angle light scattering (MALS) and viscosity detectors provide data for a cyclic topology. Cyclic polymers have lower intrinsic viscosities and smaller hydrodynamic volumes than their linear analogs. For comparison, linear polynorbornene with high *cis* selectivity (>95%) and syndiotacticity (>95%) was synthesized using Grubbs' catalyst Ru(NHC(Ad)(Mes))(=CH(PhO^{i}Pr))-(η^2-NO_3) (**15**).[58,59]

Consistent with their smaller hydrodynamic volume, a plot of log of molar mass versus elution time (Figure 6) indicates

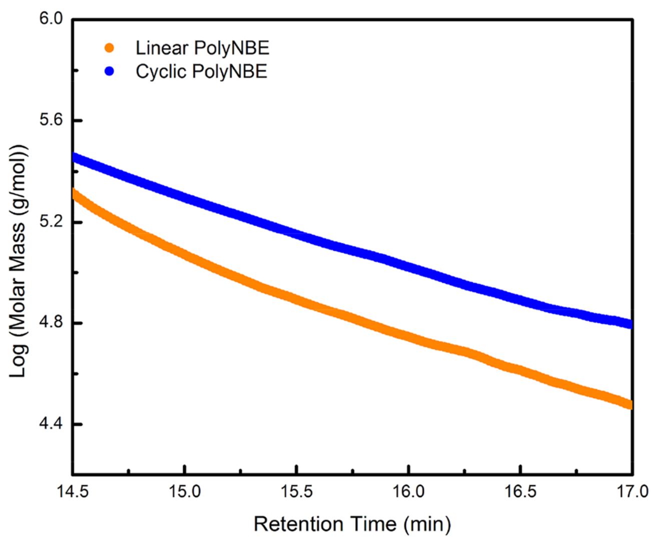

Figure 6. Log of molar mass versus elution time for polynorbornene synthesized by **6-NPh** (cyclic) and by **15** (linear).

that the cyclic polynorbornene samples with the same molar mass elute later than their linear counterparts. Confirmation of a cyclic topology also comes from a demonstration of lower intrinsic viscosities relative to the linear polymers via a Mark−Houwink−Sakurada (MHS) plot (log[η] versus log M, where [η] is the intrinsic viscosity and M is the viscosity-average molar mass) (Figure 7). The experimental ratio $[\eta]_{cyclic}/[\eta]_{linear}$ of 0.78 over a range of molecular weights is within the

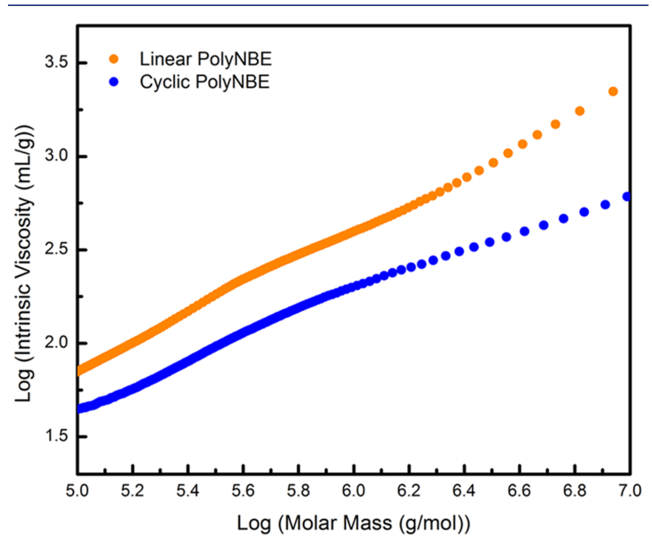

Figure 7. Log of [η] versus log of molar mass for polynorbornene synthesized by **6-NPh** (cyclic) and by **15** (linear).

https://dx.doi.org/10.1021/jacs.0c12248
J. Am. Chem. Soc. 2021, 143, 1235−1246

limits expected for the topological difference. The ratio using early predictions and under θ conditions (a = 0.5) is expected to be ~0.65,[60,61] while recent predictions suggest a ratio of 0.58 ± 0.01.[62] Experimental results are inconsistent, ranging from ~0.5 to ~0.8,[63−65] depending on molecular weight[64,66] as well as polymer-solvent systems.[63,67] For the polymers synthesized with catalysts **6-NPh** and **15**, MHS parameter a values of 0.788 and 0.700 indicate both polymers behave as flexible random coils in solution, meaning the observed differences are caused by different behavior of the polymers in solution. In addition, a plot of mean square radius of gyration ($\langle R_g^2 \rangle$) versus molar mass (Figure 8) obtained for

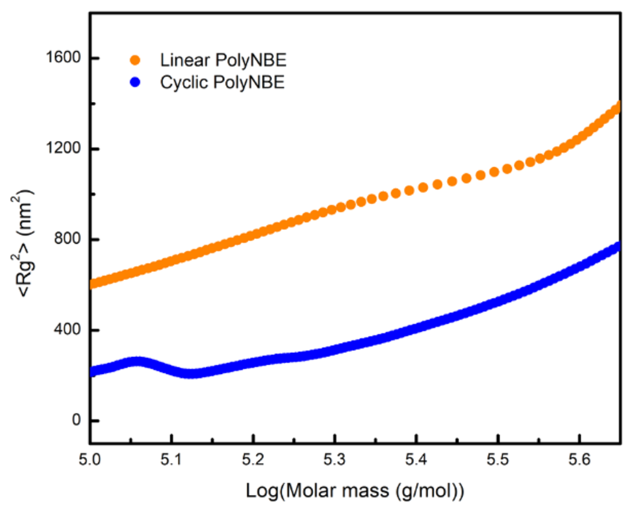

Figure 8. Plot of mean square radius ($\langle R_g^2 \rangle$) versus log of molar mass for polynorbornene synthesized by **6-NPh** (cyclic) and by **15** (linear).

cyclic and linear samples of polynorbornene provides a $\langle R_g^2 \rangle_{cyclic}/\langle R_g^2 \rangle_{linear}$ ratio of 0.48 ± 0.1, which is within the experimental error of the theoretical value of 0.5.[68,69]

CONCLUSIONS

The metal−carbon triple bond of complex **1** reacts exclusively with the C═N bond of isocyanates (R−N═C═O), leading to the formation of tethered tungsten-imido alkylidenes (**6-NR**). The standout discovery in this work is the identification and trapping of the intermediates **11-R** and **14-R** on the pathway to the formation of complexes **6-NR**. The η^2-(N,C) ligated intermediate [(O_2C^tBuC═)W(η^2-(N,C)-RNCO)-(THF)] (**11-R**) is isolable only for sterically bulky isocyanate R = ^{t}Bu prior to the formation of the final tethered tungsten-imido complex (**6-NR**), demonstrating the stability of the intermediate is sensitive to the size of the substituent. Another important finding is the loss of THF from the coordination sphere of complex **6-NR** induces decarbonylation to generate a W-ketenylide (**14-R**). In a previous paper, where the reactivity of complex **1** with CO_2 was examined, the generation of a W-ketenylide as an intermediate was proposed, but not observed.[26] This discovery provides compelling evidence for the previously proposed mechanism.

The complexes **6-NR** and **11-R** contain a tethered alkylidene and are active REMP catalysts for the synthesis of cyclic polynorbornene. By altering the R-group on the isocyanate, we were able to evaluate the effect of the imido substituent on catalyst efficiency in REMP. The tethered tungsten-imido alkylidenes (**6-NR**) successfully generate stereoregular cyclic polynorbornene. The polymerization activity of tethered tungsten-imido alkylidenes (**6-NR**) significantly depends on the lability of THF. The activity increases in the order R = Cy < Ph < ^{t}Bu. The activity decreased considerably upon the addition of 1 equiv of THF, an observation that strongly supports the previously proposed catalytic cycle where the catalyst is activated by substitution of THF from the tungsten center, followed by [2 + 2] cycloaddition of norbornene with the metal−carbon double bond.[26,27] Upon comparing the polymerization activity of **6-N^{t}Bu** relative to **11-^{t}Bu**, the latter was found to be more active and selective, likely due to additional strain present in the tethered alkylidene and greater lability of THF. Another trend observed is that increasing [monomer]:[catalyst] ratio leads to lower yields. This may be due to the increased viscosity of the reaction solution. Variable dispersities are also likely due to variations in reaction medium viscosity, with some reactions dramatically increasing in viscosity immediately upon polymerization onset. Finally, comparing the polymers produced by catalyst **6-NR** and **11-^{t}Bu** against *cis* and syndiotactic linear analogs permits their conclusive assignment as cyclic polymers. Pure tacticity in polymers imparts important materials properties. Now available in >99% syndiotacticity and >99% *cis* double bonds, future work will center on exploiting the cyclic topology in comparison to commercially produced linear polynorbornene and its hydrogenated derivative.

Several exciting applications are now available to explore for both polynorbornene and its saturated derivative in combination with stereo and topological control. Polynorbornene and its elastomer formulations are super absorbent materials and have good noise/vibration dampening properties and low friction coefficients, and are employed in automobile parts, oil absorption, sports equipment, transmission belts, ballistics jackets, and tires. Untested thus far, it will be interesting to see how the inherently different properties imparted by a lack of chain ends, such as, smaller pervaded volumes, higher packing densities, lower surface friction, and lower flow viscosities, can be exploited in end-user applications.

ASSOCIATED CONTENT

Supporting Information

The Supporting Information is available free of charge at https://pubs.acs.org/doi/10.1021/jacs.0c12248.

X-ray data for **13** (CIF)

X-ray data for **6-^{t}Bu** (CIF)

X-ray data for **6-Cy** (CIF)

X-ray data for **11-^{t}Bu** (CIF)

X-ray data for **6-Ph** (CIF)

Full experimental procedures, NMR spectra, and X-ray crystallographic and GC-MS data (PDF)

AUTHOR INFORMATION

Corresponding Author

Adam S. Veige − *Department of Chemistry, Center for Catalysis, University of Florida, Gainesville, Florida 32611, United States; George and Josephine Butler Polymer Research Laboratory, Center for Macromolecular Science and Engineering, University of Florida, Gainesville, Florida 32611, United States;* orcid.org/0000-0002-7020-9251; Email: veige@chem.ufl.edu

https://dx.doi.org/10.1021/jacs.0c12248
J. Am. Chem. Soc. 2021, 143, 1235−1246

Authors

Vineet Jakhar − *Department of Chemistry, Center for Catalysis, University of Florida, Gainesville, Florida 32611, United States*

Digvijayee Pal − *George and Josephine Butler Polymer Research Laboratory, Center for Macromolecular Science and Engineering, University of Florida, Gainesville, Florida 32611, United States*

Ion Ghiviriga − *Department of Chemistry, Center for Catalysis, University of Florida, Gainesville, Florida 32611, United States;* orcid.org/0000-0001-5812-5170

Khalil A. Abboud − *Department of Chemistry, Center for Catalysis, University of Florida, Gainesville, Florida 32611, United States*

Daniel W. Lester − *Polymer Characterization Research Technology Platform, University of Warwick, Coventry CV4 7AL, United Kingdom*

Brent S. Sumerlin − *George and Josephine Butler Polymer Research Laboratory, Center for Macromolecular Science and Engineering, University of Florida, Gainesville, Florida 32611, United States;* orcid.org/0000-0001-5749-5444

Complete contact information is available at: https://pubs.acs.org/10.1021/jacs.0c12248

Notes

The authors declare no competing financial interest.

■ ACKNOWLEDGMENTS

This material is based upon work supported by the National Science Foundation CHE-1265993 (A.S.V.). The GC/EI-MS instrument is funded by NIH S10 OD021758-01A1. K.A.A. acknowledges the NSF (CHE-1828064) and UF for the purchase of X-ray equipment. A portion of this work was performed in the McKnight Brain Institute at the National High Magnetic Field Laboratory's AMRIS Facility. The assistance of Dr. Anil Mehta in the collection of the solid-state NMR is gratefully acknowledged. The solid-state NMR study was supported by National Science Foundation cooperative agreement no. DMR-1644779 and the State of Florida. The NMR spectrometer used to acquire the solid-state NMR spectra was funded, in part, by an NIH award, S10RR031637.

■ REFERENCES

(1) Bielawski, C. W.; Benitez, D.; Grubbs, R. H. An "Endless" Route to Cyclic Polymers. *Science* **2002**, *297* (5589), 2041−2044.

(2) Tuba, R. Synthesis of Cyclopolyolefins via Ruthenium Catalyzed Ring-Expansion Metathesis Polymerization. *Pure Appl. Chem.* **2014**, *86* (11), 1685−1693.

(3) Zhang, K.; Tew, G. N. Cyclic Polymers as a Building Block for Cyclic Brush Polymers and Gels. *React. Funct. Polym.* **2014**, *80* (1), 40−47.

(4) Boydston, A. J.; Xia, Y.; Kornfield, J. A.; Gorodetskaya, I. A.; Grubbs, R. H. Cyclic Ruthenium-Alkylidene Catalysts for Ring-Expansion Metathesis Polymerization. *J. Am. Chem. Soc.* **2008**, *130* (38), 12775−12782.

(5) Boydston, A. J.; Holcombe, T. W.; Unruh, D. A.; Fréchet, J. M. J.; Grubbs, R. H. A Direct Route to Cyclic Organic Nanostructures via Ring-Expansion Metathesis Polymerization of a Dendronized Macromonomer. *J. Am. Chem. Soc.* **2009**, *131* (15), 5388−5389.

(6) Xia, Y.; Boydston, A. J.; Grubbs, R. H. Synthesis and Direct Imaging of Ultrahigh Molecular Weight Cyclic Brush Polymers. *Angew. Chem., Int. Ed.* **2011**, *50* (26), 5882−5885.

(7) Zhang, K.; Lackey, M. A.; Wu, Y.; Tew, G. N. Universal Cyclic Polymer Templates. *J. Am. Chem. Soc.* **2011**, *133* (18), 6906−6909.

(8) Zhang, K.; Tew, G. N. Cyclic Brush Polymers by Combining Ring-Expansion Metathesis Polymerization and the "Grafting from" Technique. *ACS Macro Lett.* **2012**, *1* (5), 574−579.

(9) Zhang, K.; Zha, Y.; Peng, B.; Chen, Y.; Tew, G. N. Metallo-Supramolecular Cyclic Polymers. *J. Am. Chem. Soc.* **2013**, *135* (43), 15994−15997.

(10) Zhang, K.; Lackey, M. A.; Cui, J.; Tew, G. N. Gels Based on Cyclic Polymers. *J. Am. Chem. Soc.* **2011**, *133* (11), 4140−4148.

(11) Romio, M.; Trachsel, L.; Morgese, G.; Ramakrishna, S. N.; Spencer, N. D.; Benetti, E. M. Topological Polymer Chemistry Enters Materials Science: Expanding the Applicability of Cyclic Polymers. *ACS Macro Lett.* **2020**, *9* (7), 1024−1033.

(12) Chang, Y. A.; Waymouth, R. M. Recent Progress on the Synthesis of Cyclic Polymers via Ring-Expansion Strategies. *J. Polym. Sci., Part A: Polym. Chem.* **2017**, *55* (18), 2892−2902.

(13) Haque, F. M.; Grayson, S. M. The Synthesis, Properties and Potential Applications of Cyclic Polymers. *Nat. Chem.* **2020**, *12* (5), 433−444.

(14) Liénard, R.; De Winter, J.; Coulembier, O. Cyclic Polymers: Advances in Their Synthesis, Properties, and Biomedical Applications. *J. Polym. Sci.* **2020**, *58* (11), 1481−1502.

(15) Pal, D.; Miao, Z.; Garrison, J. B.; Veige, A. S.; Sumerlin, B. S. Ultrahigh Molecular Weight Macrocyclic Bottlebrushes via Post-Polymerization Modification of a Cyclic Polymer. *Macromolecules* **2020**, *53* (22), 9717−9724.

(16) Honda, S.; Yamamoto, T.; Tezuka, Y. Topology-Directed Control on Thermal Stability: Micelles Formed from Linear and Cyclized Amphiphilic Block Copolymers. *J. Am. Chem. Soc.* **2010**, *132* (30), 10251−10253.

(17) Honda, S.; Yamamoto, T.; Tezuka, Y. Tuneable Enhancement of the Salt and Thermal Stability of Polymeric Micelles by Cyclized Amphiphiles. *Nat. Commun.* **2013**, *4* (1), 1−9.

(18) Chen, B.; Jerger, K.; Fréchet, J. M. J.; Szoka, F. C. The Influence of Polymer Topology on Pharmacokinetics: Differences between Cyclic and Linear PEGylated Poly(Acrylic Acid) Comb Polymers. *J. Controlled Release* **2009**, *140* (3), 203−209.

(19) Wang, D.; Xiao, L.; Zhang, X.; Zhang, K.; Wang, Y. Emulsion Templating Cyclic Polymers as Microscopic Particles with Tunable Porous Morphology. *Langmuir* **2016**, *32* (6), 1460−1467.

(20) Miao, Z.; Kubo, T.; Pal, D.; Sumerlin, B. S.; Veige, A. S. pH-Responsive Water-Soluble Cyclic Polymer. *Macromolecules* **2019**, *52* (16), 6260−6265.

(21) Zhu, X.; Zhou, N.; Zhang, Z.; Sun, B.; Yang, Y.; Zhu, J.; Zhu, X. Cyclic Polymers with Pendent Carbazole Units: Enhanced Fluorescence and Redox Behavior. *Angew. Chem., Int. Ed.* **2011**, *50* (29), 6615−6618.

(22) Zhang, H.; Zhou, N.; Zhu, X.; Chen, X.; Zhang, Z.; Zhang, W.; Zhu, J.; Hu, Z.; Zhu, X. *Cyclic* Side-Chain Phenylazo Naphthalene Polymers: Enhanced Fluorescence Emission and Surface Relief Grating Formation. *Macromol. Rapid Commun.* **2012**, *33* (21), 1845−1851.

(23) Miao, Z.; Pal, D.; Niu, W.; Kubo, T.; Sumerlin, B. S.; Veige, A. S. Cyclic Poly(4-methyl-1-pentene): Efficient Catalytic Synthesis of a Transparent Cyclic Polymer. *Macromolecules* **2020**, *53* (18), 7774−7782.

(24) Niu, W.; Gonsales, S. A.; Kubo, T.; Bentz, K. C.; Pal, D.; Savin, D. A.; Sumerlin, B. S.; Veige, A. S. Polypropylene: Now Available without Chain Ends. *Chem.* **2019**, *5* (1), 237−244.

(25) Morgese, G.; Trachsel, L.; Romio, M.; Divandari, M.; Ramakrishna, S. N.; Benetti, E. M. Topological Polymer Chemistry Enters Surface Science: Linear versus Cyclic Polymer Brushes. *Angew. Chem.* **2016**, *128* (50), 15812−15817.

(26) Gonsales, S. A.; Kubo, T.; Flint, M. K.; Abboud, K. A.; Sumerlin, B. S.; Veige, A. S. Highly Tactic Cyclic Polynorbornene: Stereoselective Ring Expansion Metathesis Polymerization of Norbornene Catalyzed by a New Tethered Tungsten-Alkylidene Catalyst. *J. Am. Chem. Soc.* **2016**, *138* (15), 4996−4999.

https://dx.doi.org/10.1021/jacs.0c12248
J. Am. Chem. Soc. 2021, 143, 1235−1246

(27) Nadif, S. S.; Kubo, T.; Gonsales, S. A.; VenkatRamani, S.; Ghiviriga, I.; Sumerlin, B. S.; Veige, A. S. Introducing "Ynene" Metathesis: Ring-Expansion Metathesis Polymerization Leads to Highly Cis and Syndiotactic Cyclic Polymers of Norbornene. *J. Am. Chem. Soc.* **2016**, *138* (20), 6408−6411.

(28) Peryshkov, D. V.; Schrock, R. R.; Takase, M. K.; Müller, P.; Hoveyda, A. H. *Z*-Selective Olefin Metathesis Reactions Promoted by Tungsten Oxo Alkylidene Complexes. *J. Am. Chem. Soc.* **2011**, *133* (51), 20754−20757.

(29) Sarkar, S.; McGowan, K. P.; Kuppuswamy, S.; Ghiviriga, I.; Abboud, K. A.; Veige, A. S. An OCO^{3-} Trianionic Pincer Tungsten(VI) Alkylidyne: Rational Design of a Highly Active Alkyne Polymerization Catalyst. *J. Am. Chem. Soc.* **2012**, *134* (10), 4509−4512.

(30) Gonsales, S. A.; Ghiviriga, I.; Abboud, K. A.; Veige, A. S. Carbon Dioxide Cleavage across a Tungsten-Alkylidyne Bearing a Trianionic Pincer-Type Ligand. *Dalt. Trans.* **2016**, *45* (40), 15783−15785.

(31) Weiss, K.; Schubert, U.; Schrock, R. R. Metathesis-like Reaction of a Tungsten Alkylidyne Complex with Cyclohexyl Isocyanate. *Organometallics* **1986**, *5* (2), 397−398.

(32) Luo, Y. R. *Handbook of Bond Dissociation Energies in Organic Compounds*; CRC Press: Boca Raton, FL, 2002.

(33) Galbraith, J. M.; Blank, E.; Shaik, S.; Hiberty, P. C. π Bonding in Second and Third Row Molecules: Testing the Strength of Linus's Blanket. *Chem. - Eur. J.* **2000**, *6* (13), 2425−2434.

(34) Brookes, N. J.; Ariafard, A.; Stranger, R.; Yates, B. F. Cleavage of Carbon Dioxide by an Iridium-Supported Fischer Carbene. A DFT Investigation. *J. Am. Chem. Soc.* **2009**, *131* (16), 5800−5808.

(35) Kurogi, T.; Pinter, B.; Mindiola, D. J. Methylidyne Transfer Reactions with Niobium. *Organometallics* **2018**, *37* (20), 3385−3388.

(36) Yonke, B. L.; Reeds, J. P.; Fontaine, P. P.; Zavalij, P. Y.; Sita, L. R. Catalytic Production of Isocyanates via Orthogonal Atom and Group Transfers Employing a Shared Formal Group 6 M(II)/M(IV) Redox Cycle. *Organometallics* **2014**, *33* (13), 3239−3242.

(37) McGowan, K. P.; O'Reilly, M. E.; Ghiviriga, I.; Abboud, K. A.; Veige, A. S. Compelling Mechanistic Data and Identification of the Active Species in Tungsten-Catalyzed Alkyne Polymerizations: Conversion of a Trianionic Pincer into a New *Tetraanionic* Pincer-Type Ligand. *Chem. Sci.* **2013**, *4* (3), 1145−1155.

(38) Roland, C. D.; Li, H.; Abboud, K. A.; Wagener, K. B.; Veige, A. S. Cyclic Polymers from Alkynes. *Nat. Chem.* **2016**, *8* (8), 791−796.

(39) Roland, C. D.; Zhang, T.; Venkatramani, S.; Ghiviriga, I.; Veige, A. S. A Catalytically Relevant Intermediate in the Synthesis of Cyclic Polymers from Alkynes. *Chem. Commun.* **2019**, *55* (91), 13697−13700.

(40) Roland, C. D.; Venkatramani, S.; Jakhar, V. K.; Ghiviriga, I.; Abboud, K. A.; Veige, A. S. Synthesis and Characterization of a Molybdenum Alkylidyne Supported by a Trianionic OCO^{3-} Pincer Ligand. *Organometallics* **2018**, *37* (23), 4500−4505.

(41) Carden, R. G.; Ohane, J. J.; Pike, R. D.; Graham, P. M. Synthesis of Tungsten and Molybdenum Carbon Dioxide Complexes. *Organometallics* **2013**, *32* (9), 2505−2508.

(42) Gusev, A. I.; Chuklanova, E. B.; Zhdanov, A. S.; Muzovskaya, E. V.; Kozyukov, V. P. Crystal and Molecular Structure of Trimethylsilyl Isocyanate. *J. Struct. Chem.* **1989**, *30* (5), 853−856.

(43) Kloppenburg, L.; Petersen, J. L. Facile Conversion of an Appended Silylamido to a Silyloxy Ligand via Isocyanate Elimination. Synthesis of $\{[(C_5Me_4)SiMe_2O]Zr(\eta^2\text{-}O_2CMe)(\mu\text{-}O_2CMe)\}_2$ via the Carboxylation of $[(C_5Me_4)SiMe_2(N\text{-}t\text{-}Bu)]ZrMe_2$. *Organometallics* **1996**, *15* (1), 7−9.

(44) Addison, A. W.; Rao, T. N.; Reedijk, J.; Van Rijn, J.; Verschoor, G. C. Synthesis, Structure, and Spectroscopic Properties of Copper(II) Compounds Containing Nitrogen-Sulphur Donor Ligands; the Crystal and Molecular Structure of aqua[1,7-bis(*N*-methylbenzimidazol-2′-yl)-2,6-dithiaheptane]copper(II) perchlorate. *J. Chem. Soc., Dalton Trans.* **1984**, *0* (7), 1349−1356.

(45) Messinis, A. M.; Wright, W. R. H.; Batsanov, A. S.; Howard, J. A. K.; Hanton, M. J.; Dyer, P. W. Exploration of Homogeneous Ethylene Dimerization Mediated by Tungsten Mono(Imido) Complexes. *ACS Catal.* **2018**, *8* (12), 11235−11248.

(46) Fischer, E. O.; Filippou, A. C.; Alt, H. G.; Thewalt, U. Synthesis of $[Et_2N\text{-}C{\equiv}W(CO)_2(\mu\text{-}PPh_2)_2Mo(CO)_4]^{\ominus}$, the First Anionic Carbynemetal Complex; Addition of CO_2 to the W≡C Bond. *Angew. Chem., Int. Ed. Engl.* **1985**, *24* (3), 203−205.

(47) O'Reilly, M. E.; Ghiviriga, I.; Abboud, K. A.; Veige, A. S. A New ONO^{3-} Trianionic Pincer-Type Ligand for Generating Highly Nucleophilic Metal-Carbon Multiple Bonds. *J. Am. Chem. Soc.* **2012**, *134* (27), 11185−11195.

(48) Gonsales, S. A.; Pascualini, M. E.; Ghiviriga, I.; Abboud, K. A.; Veige, A. S. Fast "Wittig-like" Reactions as a Consequence of the Inorganic Enamine Effect. *J. Am. Chem. Soc.* **2015**, *137* (14), 4840−4845.

(49) Huang, W.; Fang, D.; Temple, K.; Tidwell, T. T. Stabilized and Persistent Allenylketenes. *J. Am. Chem. Soc.* **1997**, *119* (12), 2832−2838.

(50) Lavallo, V.; Canac, Y.; Donnadieu, B.; Schoeller, W. W.; Bertrand, G. CO Fixation to Stable Acyclic and Cyclic Alkyl Amino Carbenes: Stable Amino Ketenes with a Small HOMO−LUMO Gap. *Angew. Chem., Int. Ed.* **2006**, *45* (21), 3488−3491.

(51) Stang, P. J.; Roberts, K. A. Generation and Trapping of Alkynolates from Alkynyl Tosylates: Formation of Siloxyalkynes and Ketenes. *J. Am. Chem. Soc.* **1986**, *108* (22), 7125−7127.

(52) Firl, J.; Runge, W. ^{13}C-NMR Spectrum of Ketene. *Angew. Chem., Int. Ed. Engl.* **1973**, *12* (8), 668−669.

(53) McConville, D. H.; Wolf, J. R.; Schrock, R. R. Synthesis of Chiral Molybdenum ROMP Initiators and all-cis Highly Tactic poly(2,3-(R)2norbornadiene) (R = CF_3 or CO_2Me). *J. Am. Chem. Soc.* **1993**, *115* (10), 4413−4414.

(54) Flook, M. M.; Jiang, A. J.; Schrock, R. R.; Müller, P.; Hoveyda, A. H. *Z*-Selective Olefin Metathesis Processes Catalyzed by a Molybdenum Hexaisopropylterphenoxide Monopyrrolide Complex. *J. Am. Chem. Soc.* **2009**, *131* (23), 7962−7963.

(55) Autenrieth, B.; Schrock, R. R. Stereospecific Ring-Opening Metathesis Polymerization (ROMP) of Norbornene and Tetracyclododecene by Mo and W Initiators. *Macromolecules* **2015**, *48* (8), 2493−2503.

(56) Hyvl, J.; Autenrieth, B.; Schrock, R. R. Proof of Tacticity of Stereoregular ROMP Polymers through Post Polymerization Modification. *Macromolecules* **2015**, *48* (9), 3148−3152.

(57) Dumas, A.; Tarrieu, R.; Vives, T.; Roisnel, T.; Dorcet, V.; Baslé, O.; Mauduit, M. A Versatile and Highly *Z*-Selective Olefin Metathesis Ruthenium Catalyst Based on a Readily Accessible *N*-Heterocyclic Carbene. *ACS Catal.* **2018**, *8* (4), 3257−3262.

(58) Keitz, B. K.; Fedorov, A.; Grubbs, R. H. Cis-Selective Ring-Opening Metathesis Polymerization with Ruthenium Catalysts. *J. Am. Chem. Soc.* **2012**, *134* (4), 2040−2043.

(59) Rosebrugh, L. E.; Ahmed, T. S.; Marx, V. M.; Hartung, J.; Liu, P.; López, J. G.; Houk, K. N.; Grubbs, R. H. Probing Stereoselectivity in Ring-Opening Metathesis Polymerization Mediated by Cyclometalated Ruthenium-Based Catalysts: A Combined Experimental and Computational Study. *J. Am. Chem. Soc.* **2016**, *138* (4), 1394−1405.

(60) Bloomfield, V.; Zimm, B. H. Viscosity, Sedimentation, *et Cetera*, of Ring- and Straight-Chain Polymers in Dilute Solution. *J. Chem. Phys.* **1966**, *44* (1), 315−323.

(61) Fukatsu, M.; Kurata, M. Hydrodynamic Properties of Flexible-Ring Macromolecules. *J. Chem. Phys.* **1966**, *44* (12), 4539−4545.

(62) Rubio, A. M.; Freire, J. J.; Bishop, M.; Clarke, J. H. R. Θ State, Transition Curves, and Conformational Properties of Cyclic Chains. *Macromolecules* **1995**, *28* (7), 2240−2246.

(63) McKenna, G. B.; Hadziioannou, G.; Lutz, P.; Hild, G.; Strazielle, C.; Straupe, C.; Rempp, P.; Kovacs, A. J. Dilute Solution Characterization of Cyclic Polystyrene Molecules and Their Zero-Shear Viscosity in the Melt. *Macromolecules* **1987**, *20* (3), 498−512.

(64) Roovers, J. Dilute-Solution Properties of Ring Polystyrenes. *J. Polym. Sci., Polym. Phys. Ed.* **1985**, *23* (6), 1117−1126.

(65) Jeong, Y.; Jin, Y.; Chang, T.; Uhlik, F.; Roovers, J. Intrinsic Viscosity of Cyclic Polystyrene. *Macromolecules* **2017**, *50* (19), 7770−7776.
(66) Geiser, D.; Höcker, H. Synthesis and Investigation of Macrocyclic Polystyrene. *Macromolecules* **1980**, *13* (3), 653−656.
(67) Lutz, P.; McKenna, G.; Rempp, P.; Strazielle, C. Solution Properties of Ring-shaped Polystyrenes. *Makromol. Chem., Rapid Commun.* **1986**, *7* (9), 599−605.
(68) Semlyen, J. A. *Cyclic Polymers*; Kluwer Academic Publishers: New York, 2000.
(69) Zimm, B. H.; Stockmayer, W. H. The Dimensions of Chain Molecules Containing Branches and Rings. *J. Chem. Phys.* **1949**, *17* (12), 1301−1314.

https://dx.doi.org/10.1021/jacs.0c12248
J. Am. Chem. Soc. 2021, 143, 1235−1246